frontiers in Marine Science

ORIGINAL RESEARCH
published: 20 March 2020
doi: 10.3389/fmars.2020.00045

Investigation of Siderophore-Promoted and Reductive Dissolution of Dust in Marine Microenvironments Such as *Trichodesmium* Colonies

Nivi Kessler[1,2], Stephan M. Kraemer[3], Yeala Shaked[2,4] and Walter D. C. Schenkeveld[3†]*

[1] Department of Plant and Environmental Sciences, The Alexander Silberman Institute of Life Sciences, The Hebrew University of Jerusalem, Jerusalem, Israel, [2] The Fredy and Nadine Herrmann Institute of Earth Sciences, The Hebrew University of Jerusalem, Jerusalem, Israel, [3] Department of Environmental Geosciences, University of Vienna, Vienna, Austria, [4] Interuniversity Institute for Marine Sciences, Eilat, Israel

OPEN ACCESS

Edited by:
Christel Hassler, Université de Genève, Switzerland

Reviewed by:
Sylvia Gertrud Sander, University of Otago, New Zealand
Daniel James Repeta, Woods Hole Oceanographic Institution, United States

***Correspondence:**
Yeala Shaked
yeala.shaked@mail.huji.ac.il

†Present address:
Walter D. C. Schenkeveld, Copernicus Institute of Sustainable Development, Faculty of Geosciences, Utrecht University, Utrecht, Netherlands

Specialty section:
This article was submitted to Marine Biogeochemistry, a section of the journal Frontiers in Marine Science

Received: *14 August 2019*
Accepted: *23 January 2020*
Published: *20 March 2020*

Citation:
Kessler N, Kraemer SM, Shaked Y and Schenkeveld WDC (2020) Investigation of Siderophore-Promoted and Reductive Dissolution of Dust in Marine Microenvironments Such as Trichodesmium Colonies. Front. Mar. Sci. 7:45. doi: 10.3389/fmars.2020.00045

Desert dust is a major source of iron (Fe) to phytoplankton in many Fe-poor ocean regions. However, phytoplankton often struggle to obtain dust-bound Fe (dust-Fe) due to its low solubility and short residence time in the euphotic zone. *Trichodesmium*, a globally important nitrogen-fixing, cyanobacterium, is uniquely adapted for utilizing dust as a source of Fe. *Trichodesmium* colonies can actively collect and concentrate dust particles within the colony core and enhance dust-Fe dissolution rates via two bio-dissolution mechanisms: reduction and complexation by strong Fe-chelators termed siderophores. Here, mimicking bio-dissolution in *Trichodesmium* colonies, we studied the kinetics of desert dust dissolution by a siderophore and a reductant in seawater. By concurrent measurements of dissolved Fe, silica (Si), and aluminum (Al) we recognized two major mineral pools that released Fe into seawater over an 8-day period: Fe(hydr)oxides and aluminosilicates. In the presence of the siderophore desferrioxamine-B, we observed two stages of dissolution: a short stage of fast Fe dissolution followed by a lasting stage of slow Fe dissolution that was highly correlated to Al and Si dissolution. In the presence of the reductant, ascorbate, Fe dissolution was not correlated to Al and Si dissolution and was relatively slow. Based on these observations and on dust mineralogy, we constructed a conceptual model for dust-Fe dissolution by a siderophore and a reductant from two major mineral pools: reductive and siderophore-promoted dissolution of Fe(hydr)oxides and slow continuous dissolution of Fe-bearing clays in the presence of a siderophore. Our findings highlight the importance of clays as an Fe source to *Trichodesmium* and possibly to other marine phytoplankton and can be further used to assess the contribution of dust to the Fe requirements of natural *Trichodesmium* colonies. Combining our measured bio-dissolution rates with dust concentrations retained within colonies from the Gulf of Aqaba, we calculated the supply of dissolved Fe from dust to single *Trichodesmium* colonies. Applying published

Fe-quotas and growth rates we calculated the Fe requirements of the colonies under Fe-limited and Fe-replete conditions. The calculated dissolved Fe supply from dust retained within colonies can fulfill the Fe requirements of slow growing Fe-limited colonies, but cannot support fast growth and/or higher cellular Fe quotas. We conclude that despite these bio-dissolution mechanisms, dust-Fe availability to *Trichodesmium* is low and propose that it employs additional mechanisms to actively mine Fe from dust.

Keywords: bioavailability, iron, dissolution kinetics, ligands, reduction, siderophore, trichodesmium, dust

INTRODUCTION

Iron (Fe) is an essential trace nutrient, required for a wide range of enzymatic processes, including photosynthesis and nitrogen fixation (Morel and Price, 2003). The low solubility of Fe in oxygenated, circumneutral pH waters results in sub-nanomolar concentrations of dissolved Fe in oceanic surface water (Byrne and Kester, 1976; Jolivet et al., 2004). Thus, the scarcity of dissolved Fe limits phytoplankton productivity and nitrogen fixation rates across vast oceanic regions (Martin et al., 1991; Sohm et al., 2011; Moore et al., 2013; Tagliabue et al., 2017). Atmospheric dust is considered an important source of Fe to remote, Fe-poor ocean regions (Jickells et al., 2005; Conway and John, 2014). However, slow dissolution of Fe-bearing minerals in dust and sinking of dust particles out of the photic zone restrict the utilization of dust-bound Fe (dust-Fe) by marine microorganisms such as phytoplankton and bacteria (Boyd et al., 2010).

The cyanobacterium *Trichodesmium* spp. is an important ecosystem player in oligotrophic ocean regions, which contributes up to ∼50% of marine nitrogen fixation and forms extensive surface blooms visible even from space (Carpenter et al., 1992; Westberry and Siegel, 2006). Maintaining the enzymatic machinery required for nitrogen fixation raises *Trichodesmium*'s Fe requirements, resulting in cellular Fe quotas that exceed other oceanic phytoplankton by ∼10-fold (Berman-Frank et al., 2001; Kustka et al., 2003; Nuester et al., 2012). Accumulating research indicates that *Trichodesmium* is especially adapted to utilize dust as a source of Fe (Rueter et al., 1992; Tovar-Sanchez et al., 2006; Rubin et al., 2011; Langlois et al., 2012; Basu and Shaked, 2018; Polyviou et al., 2018; Basu et al., 2019; Eichner et al., 2019a,b; Gledhill et al., 2019; Kessler et al., 2019). *Trichodesmium* employs different strategies to overcome the physical constraints on dust-Fe acquisition: dust sinking to depth and loss of attached particles. By adjusting its buoyancy and staying near the surface, *Trichodesmium* increases its encounter rate with dust deposited on the ocean surface (Walsby, 1978; Villareal and Carpenter, 2003). *Trichodesmium* forms relatively large and intricate colonies that efficiently trap dust particles and shuffle them to the core of the colony (Rubin et al., 2011; Rueter et al., 1992; Langlois et al., 2012; Bif and Yunes, 2017).

Trichodesmium colonies can also accelerate the dissolution rate of Fe from the Fe(hydr)oxides and dust particles that they collect (Rubin et al., 2011; Basu and Shaked, 2018). The pathways for this bio-enhanced dissolution are still under investigation, but there is evidence suggesting that *Trichodesmium* colonies employ two bio-dissolution mechanisms: siderophore promoted dissolution and reductive dissolution. Siderophores are low molecular weight organic ligands with a high affinity for Fe, secreted mostly by heterotrophic bacteria (Trick, 1989; Granger and Price, 1999; Rosenberg and Maurice, 2003). Siderophores enhance Fe dissolution rates by forming a surface complex with Fe atoms exposed at the mineral surface, facilitating the breaking of the bonds with the mineral lattice and carrying the Fe into solution as Fe(III)-siderophore complexes (Kraemer et al., 2005). In a recent study, our group showed that heterotrophic bacteria, naturally residing in *Trichodesmium* colonies, secrete the ferrioxamine siderophores B (DFOB), E, and G (Gledhill et al., 2019). Furthermore, the secretion of the siderophores was found to be stimulated by dust inputs, suggestive of a mutualistic pathway for increasing the supply of Fe from dust (Basu et al., 2019).

Biological reduction of mineral-Fe occurs by cell surface-bound reductases or via release of Fe-reducing compounds into the surrounding milieu (Whooley and McLoughlin, 1982; Hernandez, 2001; Kuhn et al., 2013). In reductive dissolution, conversion of mineral Fe(III) to more soluble Fe(II) facilitates detachment and accelerates dissolution (Suter et al., 1991). Although there is no direct evidence of reductive dissolution by *Trichodesmium*, its ability to reduce dissolved Fe prior to uptake suggests that it can also reduce Fe at the mineral surface (Roe and Barbeau, 2014; Lis et al., 2015; Eichner et al., 2019a,b).

In this study we aim to chemically characterize the dissolution of dust by nutrient acquisition strategies employed by *Trichodesmium*. Studying bio-dissolution of dust-Fe by *Trichodesmium*, and marine organisms in general, is a challenging task. First, dissolution rates of dust-Fe and Fe solubility are exceptionally low in seawater resulting in very low dissolved Fe concentrations, which are analytically challenging to measure (Liu and Millero, 2002). Second, dust is a complex matrix, composed of a heterogeneous particle mixture with varying size, mineralogy and Fe contents, making it difficult to obtain a mechanistic understanding. To overcome these challenges, many studies, including several by our own group, substituted dust with well-defined and well-characterized minerals, such as ferrihydrite and hematite (for example: Kuma and Matsunaga, 1995; Nodwell and Price, 2001; Yoshida et al., 2002; Wang et al., 2015; Kranzler et al., 2016; Basu and Shaked, 2018). Another commonly used approach is examining dust dissolution in conditions that are more favorable for Fe dissolution, such as at low pH or at low ionic-strength solutions (Spokes and Jickells, 1996; Borer et al., 2005; Aguilar-Islas et al., 2010). Although such experimental setups have greatly advanced

our understanding of mineral Fe dissolution, they may fail to provide insight in important components of the process under natural marine conditions.

To mimic *Trichodesmium* mediated dissolution of dust-Fe, we incubated desert dust in seawater in the presence of the siderophore DFOB (SD – siderophore-promoted dissolution) and the reductant ascorbate (RD – reductive dissolution). During 1-week-long dissolution experiments, we periodically measured the dissolved concentrations of Fe, aluminum (Al), and silica (Si). Combining the dissolution kinetics of these elements with dust mineralogy we constructed a conceptual model for the dissolution of dust-Fe by the two examined biological mechanisms. We recognized two dominant Fe-pools: (1) Fe(hydr)oxides that undergo fast SD and slower RD and (2) Fe-bearing clays that undergo SD and contribute a slow and steady flux of dissolved Fe. From the measured Fe dissolution rates, we calculated Fe supply rates from dust retained within a *Trichodesmium* colony. Comparing the supply rates to the Fe requirements of *Trichodesmium*, we find that these calculated rates can fulfill the Fe requirements of slow-growing Fe-limited colonies, but cannot support fast growth and/or higher cellular Fe quotas.

MATERIALS AND METHODS

Dust Collection and Characterization

Desert dust was collected at the northern edge of the Gulf of Aqaba, at the Interuniversity Institute of Marine Sciences (IUI) in Eilat (see detailed location in Chen et al., 2007). This site receives high loads of dust originating from the Sahara and the Arabian Peninsula (Chen et al., 2007, 2008; Torfstein et al., 2017). This dust is the major source of mineral particles to the surface water of the Gulf (Torfstein et al., 2017) and probably to *Trichodesmium* colonies that prevail in these waters in spring and autumn (Rubin et al., 2011; Basu and Shaked, 2018; Basu et al., 2019; Kessler et al., 2019).

Dust collection was conducted over a period of several weeks, using a home-made static PVC aerosol collection device. The device was placed horizontally in front of a vertical wall to enable settling of the dust. The dust was sieved through a 200 μM mesh and stored in a desiccator. A detailed chemical and physical characterization of the dust is presented in section "Dust Characterization."

The mineralogical composition of the dust was analyzed by X-ray diffraction (XRD), using a Bruker X-ray Diffractometer (AXS D8 Advance). The dust was analyzed once in its pristine form and once after an acid wash (24 h incubation in 4 M acetic acid), which removes carbonate minerals and allows a more detailed analysis of the aluminosilicates. The relative abundance of the minerals was calculated using the Rietveld analysis, a systematic procedure for decomposing a powder pattern into its components by calibration of diffraction model parameters including peak width and shape (Young, 1993).

The size, spatial arrangement and local elemental composition of the dust particles were analyzed using scanning electron microscopy (SEM). The dry dust was placed directly on a carbon conductive adhesive tape and coated with gold. The analysis was conducted using a high-resolution SEM equipped with energy dispersive X-ray spectroscopy (EDS; Sirion). The size distribution of the dust particles was analyzed using ImageJ software. Elliptical shapes were fitted manually to particles and the area was measured by a built-in function. The equivalent diameter of the fitted ellipses was extracted from the measured area (A) according to: $\text{Diameter}_{eq} = 2\sqrt{(A/\pi)}$.

The amorphous Fe(hydr)oxides content of the dust was estimated with an ammonium oxalate extraction, following the procedure in Schwertmann (1964). The total Fe content in the dust was estimated to be 3.5%, a value widely used in assessing global−scale Fe inputs to the ocean (Duce and Tindale, 1991).

Experimental Setup and Rationale

The experiments were designed to explore bio-dissolution processes that occur within *Trichodesmium* colonies, and hence dust dissolution kinetics were examined in Synthetic Ocean Water (SOW) in the presence of the siderophore DFOB and the reductant ascorbate. Batch experiments with 0.3 g L^{-1} dust suspensions were carried out for 8 days and dissolution rates were evaluated from the accumulation of dissolved Fe, Al, and Si over time.

The chosen dust concentration is higher than that found in seawater, but well within the range found in *Trichodesmium* colonies (see section "Estimation of Dust Loads on *Trichodesmium* Colonies"). The experiment length was set to 8 days to account for the limited longevity of *Trichodesmium* colonies. The chosen siderophore was DFOB, a ferrioxamine siderophore that is frequently detected in surface waters and is, hence, considered important for the marine Fe-cycle (Boiteau et al., 2016; Velasquez et al., 2016; Frischkorn et al., 2017). The conditional stability constants (log K_{cond}, Fe'L) of DFOB, determined in different studies, vary from 11.6 to 16.5 (Rue and Bruland, 1995; Croot and Johansson, 2000; Witter et al., 2000; Maldonado et al., 2005).

Moreover, recent incubation studies with natural *Trichodesmium* colonies from the Gulf of Aqaba measured production of 50 pM to 1.2 nM – during 1–2 days, presumably synthesized by the bacteria associated with the colonies (Basu et al., 2019; Gledhill et al., 2019). Considering the colony numbers in the incubation and a colony volume of 0.25 μl, these concentrations correspond to a maximum of 0.8 μM ferrioxamines in the colony's microenvironment. We chose to use a wide concentration range of 3–90 μM DFOB: A low concentration to stay close to *Trichodesmium*'s microenvironment and higher concentrations to examine whether dissolution is concentration dependent and to attempt to calculate the activation energy for dissolution. Ascorbate was chosen to represent bio-reduction since it was shown to reduce and solubilize the reactive Fe pool from dust that is also reducible by bacteria (Hyacinthe et al., 2006). The applied concentrations of ascorbate (10–300 μM) were set relatively high to maintain reductive activity in aerobic conditions for a prolonged period of time.

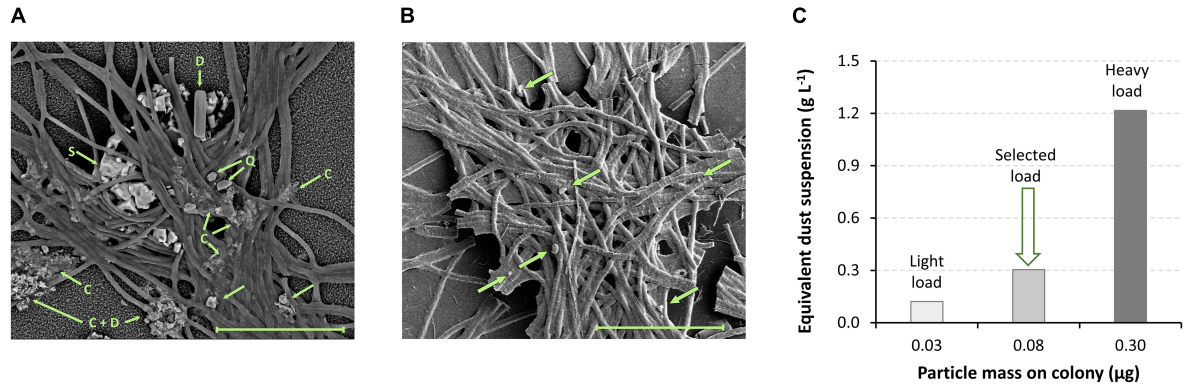

FIGURE 1 | Particle load on *Trichodesmium* colonies. Puff shaped *Trichodesmium* colonies, collected in the Gulf of Aqaba, contain variable loads of mineral particles. **(A,B)** SEM-EDS analyses of colonies collected on **(A)** July 10, 2017 and **(B)** December 9, 2014 were used to estimate the mass of particles on a colony; dust particles are marked with arrows. Colony A is heavily loaded with particles, containing numerous patches of small particles and a few larger particles; particle mass ∼0.3 μg (calculation explained in section "Estimation of Dust Loads on *Trichodesmium* Colonies"). Particles with known mineralogy are marked: C, clay/mica minerals; S, NaCl (precipitated during drying); Q, quartz; D, diatom frustule. Colony B has a light load, containing only a few single particles; particle mass ∼0.03 μg. **(C)** Equivalent particle suspensions were calculated for the heavy and light particle loads, assuming a colony volume of 0.25 μl. The dust suspension concentration of 0.3 g L^{-1}, used in this work, is equivalent to 0.08 μg of dust per colony, which lies within the range of natural observations. Scale bar = 100 μM.

Prior to addition of DFOB and ascorbate, the dust was pre-equilibrated with the SOW (up to 90% of the final suspension volume) for 16 h. Blank control treatments (without DFOB or ascorbate) were also included. Suspensions were incubated in 50 mL polypropylene centrifuge tubes that were placed in an end-over-end shaker rotating at 18 rpm in the dark, at 22°C. Aliquots of the suspensions were taken at 1, 2, 4, 8, 24, 48, 96, and 192 h after application of the treatments. Immediately after sampling, the aliquots were filtered through a 0.45 μM cellulose acetate filter, acidified with nitric acid (to a final concentration of 2%) and stored in the dark at 4°C until analysis. The solution pH was monitored throughout the incubation and was found to be stable (8.0 ± 0.2). All experiments were carried out in duplicates; error bars in **Figures 3**, **4**, **6A**, represent the error calculated from the duplicates. The experiments with 90 μM DFOB were repeated at 7, 35, and 50°C.

Samples were diluted 5× prior to analysis and metal concentrations (Fe, Al, Si, Mn, Cr, Co, Ni, Cu, Zn, Cd, and Pb) were quantified by ICP-OES (Optima 5300 DV, Perkin Elmer), to enable measuring an array of elements in a high ionic strength solution. Measuring was done using external calibration methods with certified elemental standard solutions; samples were matrix matched. Quality control samples were included after every 20th sample to monitor signal drift. The limits of quantification for Fe, Al, and Si were 5.1, 20, and 20 ppb, respectively.

Estimation of Dust Loads on *Trichodesmium* Colonies

All *Trichodesmium* puff-shaped colonies collected from the Gulf of Aqaba contained mineral particles, although particle sizes, numbers, and mass were highly variable. To assess the mass of particles on natural *Trichodesmium* colonies were collected and inspected using high-resolution imaging techniques.

Colonies were collected at the IUI pier with a 200 μM plankton net subjected to ambient currents (see details in Kessler et al., 2019). Freshly collected colonies were fixed in filtered seawater with 2% glutaraldehyde, air dried on a 0.2 μM Supor membrane filter and coated with 15–20 nM of gold, using a Hummer sputter coater (Technics). The colonies were analyzed using high resolution scanning electron microscopy (HR SEM, Sirion) equipped with energy dispersive spectroscopy (EDS) at the Hebrew University center for Nanoscience and Nanotechnology. Colony-associated patches of particles with EDS spectra of rock-forming minerals were considered as dust particles. The particle-patch area was estimated from the SEM micrographs and converted to volume by multiplying it by 10 μM (estimated penetration depth of the EDS beam). Particle-patch volume was converted to dust mass using a mean density of 2.5 g cm^{-3}.

Mineral mass calculation of colonies heavily loaded with particles (e.g., **Figure 1A**) and colonies sparsely loaded with particles (e.g. **Figure 1B**) ranged between 0.03 and 0.3 μg of mineral particles per colony. Within the colony microenvironment that has an average volume of 0.25 μl (Basu and Shaked, 2018), these particle loads are equivalent to concentrations of 0.1 and 1.2 g L^{-1} (**Figure 1C**). We hence chose to work with a particle suspension of 0.3 g L^{-1}, which lies within this range.

Data Analysis

The dissolution rates were determined by linear regression of the dissolved concentrations versus time. The rates of RD were calculated for the first five time points (1–24 h). SD rates were calculated separately for the early stage (1–8 h), and for the late stage (24–192 h). Regression lines were not forced through the origin; the positive intercepts resulted from fast initial dissolution, which is commonly observed in batch experiments and possibly arises from small amounts of labile Fe species (Kraemer et al., 2005). The elemental ratios in solution during SD were estimated by linear regression of the solution concentrations. All sampling times and all DFOB treatments were

included, except for the 3 μM DFOB treatment, in which the free-siderophore concentrations became nearly depleted during the experiment. The elemental correlations across different temperatures included only the last four timepoints (24–192 h), as this analysis refers only to the late stage of the dissolution experiments.

Medium and Reagents

Dissolution experiments were conducted in pH adjusted (pH ∼8 to 8.2) SOW, prepared according to the Aquil salt mix protocol as outlined by Morel et al. (1979). The L-ascorbic acid ($C_6H_8O_6$, Sigma-Aldrich, >95%) and desferrioxamine B mesylate salt ($C_{25}H_{48}N_6O_8{\cdot}CH_4O_3S$, DFOB, Sigma-Aldrich, >92.5%) were used as received. DFOB and ascorbate solutions were prepared freshly before each dissolution experiment. Ultrapure water (resistivity > 18.2 MΩ·cm, Milli-Q, Millipore) was used in all solution preparations. The pH of the ascorbate solution was raised to ∼8, by adding NaOH solution, to prevent acidification of the SOW-dust mixture.

RESULTS

Dust Characterization

Desert-dust collected at the northern edge of the Gulf of Aqaba was analyzed by several methods to obtain a broad characterization. Dust mineralogy was analyzed by XRD (**Table 1**). Silicates (aluminosilicates + quartz) were the largest major component, accounting for 52% of the dust mass, while carbonates and evaporates accounted for 39 and 9% of the dust mass, respectively. Within the silicates, clay minerals were the largest constituent. The three identified clay minerals were montmorillonite, kaolinite, and palygorskite. Montmorillonite was the most abundant clay mineral, accounting for 62% of the clay mass and 15% of the dust mass. The primary silicate muscovite was also abundant and accounted for 16% of the dust mass. Fe(hydr)oxides were not detected, potentially due to their low crystallinity.

TABLE 1 | The mineralogical composition of the studied dust according to an XRD analysis.

Mineral phase	W%
Calcite	31 (0.1)
Dolomite	8 (0.7)
Gypsum	6 (0.5)
Halite	3 (0.3)
Quartz	5 (0.4)
Aluminosilicates	
Albite	6 (0.1)
Clay/Mica*	
Montmorillonite	15 (0.3)
Kaolinite	6 (0.1)
Palygorskite	3 (0.6)
Muscovite	16 (0.6)
Σ Aluminosilicates	47
Σ Total	100

*referred to as "clays" in the text.

The size distribution and spatial arrangement of the dust was assessed using SEM-EDS analysis (**Figure 2**). We identified a population of small particles, which ranged from sub-micrometer to ∼15 μM in diameter. The average diameter of this particle group was 6 μM (±5 μM; n = 137). The small particles were either in aggregates (**Figure 2A**) or adhered to larger particles (**Figure 2B**) and were too small to be analyzed individually by EDS. The overall composition of the aggregates was characteristic of a mixture of clay and mica minerals (**Figure 2C**); from here on we refer to this particle population as "clays," for the sake of simplicity. A few Fe(hydr)oxide particles were also identified within the small particle aggregates, amongst them magnetite, titanium-magnetite and hematite. We speculate that the average Fe content, presented in **Figure 2C**, was affected by the presence of small Fe(hydr)oxide particles within the aggregates. In addition, there were large particles with diameters of 50–500 μM, with an average diameter of 170 ± 100 μm; n = 30). The large particles were identified by EDS as NaCl, gypsum, feldspars, carbonates, and quartz.

The amorphous Fe content of the dust, estimated by an ammonium oxalate extraction, amounted to 31 μmol Fe g^{-1} Dust (i.e., 1.7 g kg^{-1}), corresponding with 5% of the total Fe. Amorphous Fe is widely considered the Fe fraction that is available for dissolution (Kuma et al., 1996; Visser et al., 2003; Bligh and Waite, 2011). The implications of this estimate are further discussed in section "Dust-Fe Dissolution Patterns."

Dust Dissolution Kinetics in the Presence of a Siderophore and a Reductant

Background Dissolution

In the absence of ascorbate and DFOB, Fe and Al dissolution in SOW was limited by the low solubility of their corresponding hydroxide minerals at the circumneutral pH of seawater; Fe concentrations were below the detection limit and Al concentrations were on average 0.7 ± 0.4 μM (**Figure 3B**). Si concentrations were not at equilibrium with the dust mineral phases, but increased continuously (**Figure 3C**) at a rate of 2.3 μmol Si g^{-1} $Dust^{-1}$ d^{-1} (or 0.7 μM d^{-1}), in agreement with a previous assessment of dust-Si dissolution in seawater (Ganor et al., 1991).

Reductive Dissolution

Fe dissolution and accumulation in solution were promoted by ascorbate, at concentrations of 30 μM and above (**Figure 3A**). As these experiments were conducted at ambient oxygen levels, Fe(III) reduction and Fe(II) oxidation by oxygen occurred simultaneously. The reducing capacity of ascorbate, which was gradually consumed by reduction of Fe and oxygen, decreased throughout the experiment. The changing balance between Fe reduction and oxidation eventually shifted the system from net-dissolution to net-precipitation. This shift is manifested as an overturn in slope after 4 days, at 30 and 100 μM of ascorbate. Only at the largest ascorbate concentration (300 μM), did net Fe reduction persist throughout the experiment. The maximum

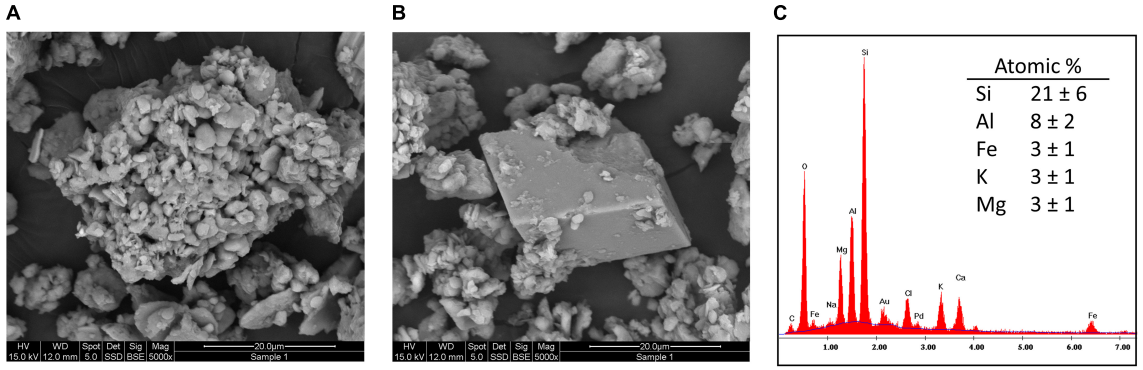

FIGURE 2 | SEM-EDS analysis of the small particle population. The small particles were observed in the form of particle aggregates **(A)** or adsorbed to large particles, such as the presented calcite particle **(B)**. A typical EDS spectrum obtained from the particle aggregates, with the average chemical composition of six analyzed aggregates, is presented in **C**.

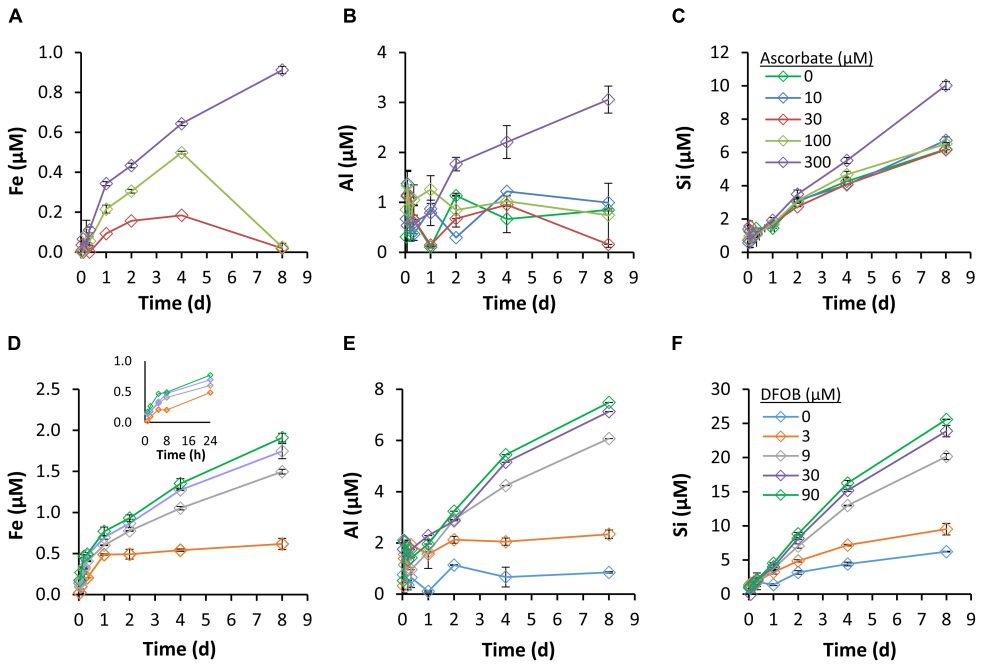

FIGURE 3 | Dissolution kinetics of Fe **(A,D)**, Al **(B,E)**, and Si **(C,F)** in the presence of ascorbate **(A–C)** and DFOB **(D–F)**. A 0.3 g dust L^{-1} dust-SOW suspension was supplemented with 3–90 µM of DFOB or 10–300 µM of ascorbate and incubated with shaking. Dissolution was monitored over a period of 8 days; the solution phase was sampled at designated time points, filtered and analyzed by ICP-OES. Iron concentrations in the 0 µM DFOB, and 0 and 10 µM ascorbate treatments were below the detection limit.

Fe concentration that was measured in the presence of ascorbate was 0.9 µM (**Figure 3A**), equivalent to 3 µmol Fe g^{-1} $Dust^{-1}$ d^{-1}, or 0.6% of the dust-Fe. Fe dissolution rates were calculated for the first 24 h, during which precipitation was minimal (**Figure 4C**). Increasing the ascorbate concentration (from 30 to 300 µM ascorbate) caused a 4-fold increase in Fe-dissolution rates (0.3 – 1.2 µmol Fe g^{-1} $Dust^{-1}$ d^{1}).

Ascorbate also enhanced the dissolution and accumulation in solution of Al and Si, but only when supplemented at the 300 µM concentration (**Figures 3B,C**). For Al, it is hard to determine whether ascorbate induced faster dissolution or merely facilitated accumulation of dissolved Al in solution. Empirical evidence suggests that the formation of aluminum-ascorbate complexes can increase the solubility of aluminum oxides (Partridge et al., 1989); for our experimental conditions this effect could support the observed accumulation of dissolved Al. For Si, for which accumulation in solution was not constrained by mineral solubility, we observed enhanced dissolution only at 300 µM of ascorbate (**Figures 3C**, **4D**). In contrast to RD of Fe, which was detectable already after 2 h, enhanced Si dissolution was detectable only after 48 h (**Figure 3C**).

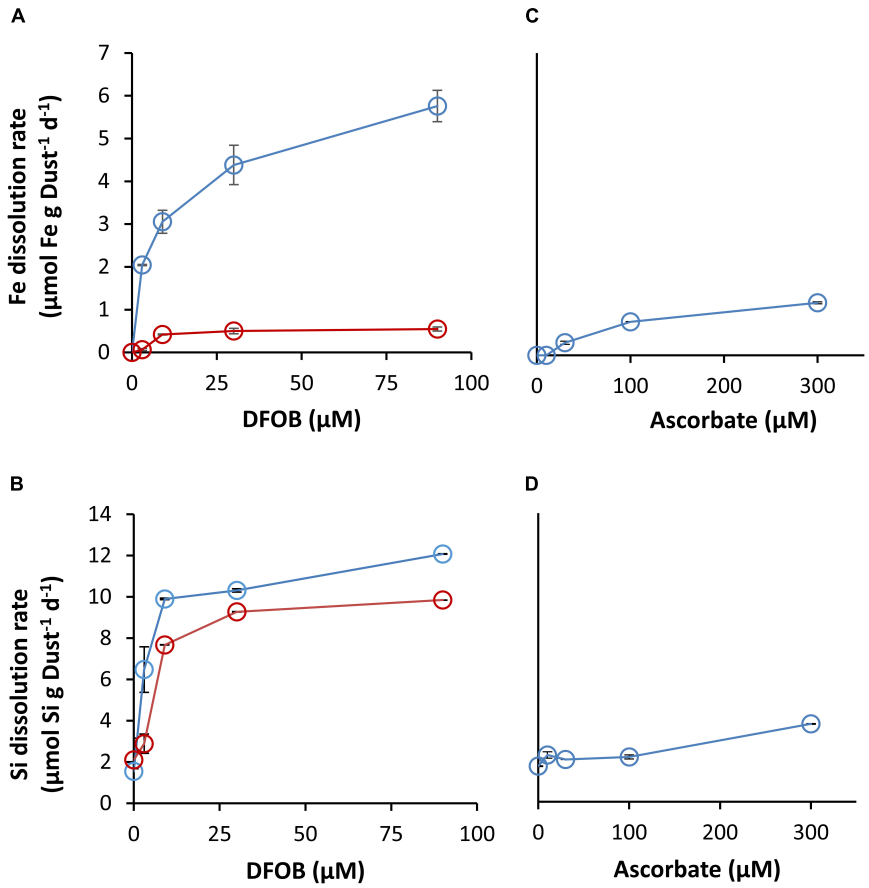

FIGURE 4 | Dissolution rates of Fe and Si from dust, as a function of applied DFOB **(A,B)** and ascorbate concentrations **(C,D)**. SD rates were calculated separately for 0–8 h (blue) and 24–192 h (red). RD rates were calculated for the first 24 h.

Siderophore-Promoted Dissolution

DFOB mobilized Fe from dust throughout the 8-day experiments (**Figure 3D**). The accumulation of dissolved Fe in solution beyond the solubility of amorphous Fe(hydr)oxide (0.3 nM; Byrne and Kester, 1976) indicates the formation of soluble Fe-DFOB complexes. The kinetics of SD had two stages: an early and fast dissolution stage that lasted until Fe concentrations reached ∼0.5 µM (by approximately 8 h; insert in **Figure 3D**), followed by a slow stage that continued until the end of the experiment. Early SD rates were strongly influenced by the supplemented DFOB concentration (**Figure 4A**), with a 180% rate increase (2.0 – 5.8 µmol Fe g^{-1} $Dust^{-1}$ d^{-1}) from 3 to 90 µM DFOB. In late SD, Fe dissolution rates were much smaller (by 7- to 10-fold) and only moderately influenced by the applied DFOB concentration, with only a 30% increase (0.42 – 0.55 µmol Fe g^{-1} $Dust^{-1}$ d^{-1}) between 9 and 90 µM DFOB (**Figure 4A**). For all DFOB applied concentrations, early SD was faster than reductive dissolution (**Figure 4**). Ultimately, DFOB solubilized up to ∼2 µM of Fe (at 90 µM DFOB), which is 3% of total Fe in the dust.

DFOB also significantly enhanced Al and Si dissolution and solubilized as much as 20 µM of Si and 7 µM of Al above the control (**Figures 3E,F**). Enhanced Al dissolution can be explained similarly as for Fe, since DFOB is known to form soluble complexes with Al(III) (Schenkeveld et al., 2016; **Figure 3E**). DFOB-enhanced Si dissolution is not as trivial since DFOB has little affinity for Si complexation (Kraemer et al., 2015) and thus cannot promote its dissolution directly. Nonetheless, the Si dissolution rate was strongly influenced by the supplemented DFOB concentration (**Figures 3F**, **4B**). In contrast to Fe, Si dissolution was relatively uniform over time. For Al, we could not determine whether the dissolution rates changed in the transition from the early to the late dissolution stage, due to a lack of trend in concentration during the first 24 h (**Figure 3E**).

In the treatment with the smallest DFOB addition (3 µM), accumulation of dissolved Fe, Si, and Al slowed down significantly after 24 h, to nearly ambient dissolution rates (i.e., rates with zero DFOB; **Figures 3D–F**). Assuming that all the dissolved Fe and Al had formed a 1:1 complex with DFOB, by 24 h ∼70% of the DFOB was complexed, and by 8 days there was no free DFOB left to complex additional metals (78% was bound to Al and 21% to Fe). Considering that some DFOB was also adsorbed onto the mineral surfaces,

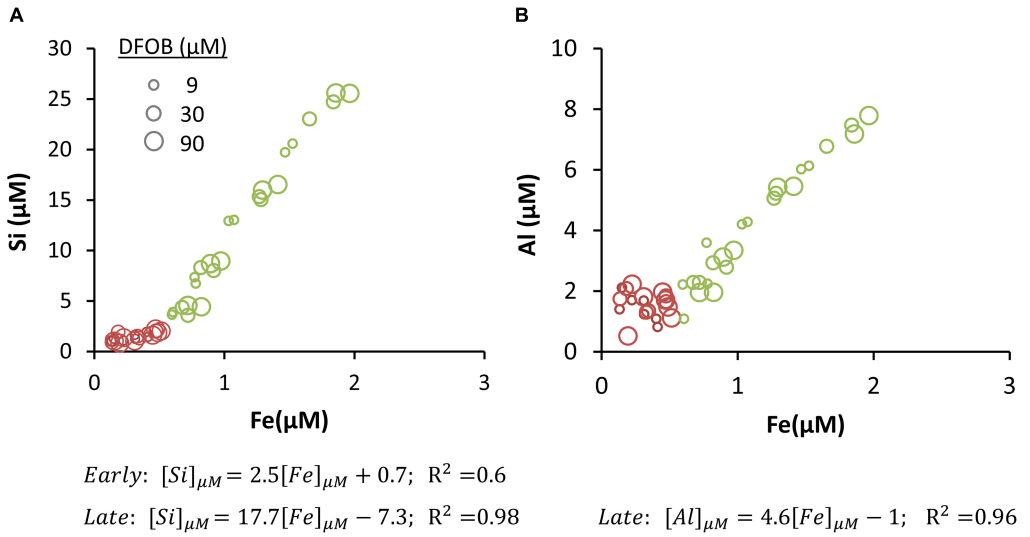

FIGURE 5 | Concentration of Si **(A)** and Al **(B)** as a function of Fe concentration. The data includes all time points from experiments with 9, 30, and 90 µM DFOB. Data from 0–8 h (Early) is presented in red and data from 24–192 h (Late) in green. The marker size indicates the applied DFOB concentration. Linear trends were fitted separately for the early and late stages and the fitting equations are presented below the graphs. The early stage correlation between Al and Fe was very weak (R^2 = 0.15) and is therefore not displayed.

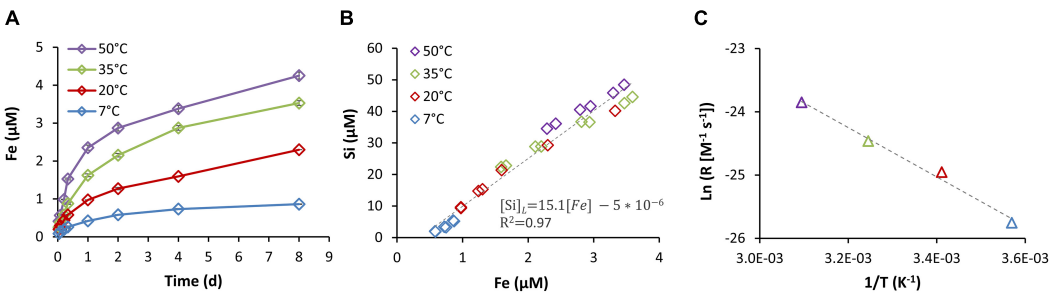

FIGURE 6 | Iron dissolution kinetics at various temperatures (7–50°C) in the presence of 90 µM DFOB **(A)**. **(B)** Late stage (24–192 h) Si concentrations as a function of Fe concentrations. **(C)** Arrhenius plot showing the natural logarithm of the dissolution rate as a function of the inverse of temperature. From the slope of the Arrhenius plot an apparent activation energy of 32.4 kJ/mol is determined.

it is safe to suggest that metal accumulation in solution was limited by free DFOB.

Correlations Between Fe, Al, and Si in the Presence of DFOB

The overall similarity in accumulation patterns of Al, Fe, and Si in solution in the presence of DFOB (**Figure 3**) may be interpreted as the result of the dissolution of a single mineral phase of which these ions are stoichiometric components. To further investigate this possibility, we carefully examined the correlations between these elements (**Figure 5**, the Al-to-Si correlation is shown in **Supplementary Figure S1**). During the late stage, Fe concentrations were strongly correlated to both Al and Si concentrations ($R^2 > 0.95$). The applied DFOB concentrations did not affect the ratio in which these elements were mobilized, even though it clearly influenced the concentration of dissolved Fe, Si, and Al (**Figure 3**).

The correlation between Fe and Si concentrations was distinctly bimodal (**Figure 5A**). At low Fe concentrations the Si/Fe slope was relatively small (2.5) and the correlation was weak (R^2 = 0.6). At ∼0.5 µM Fe, the Si/Fe correlation slope increased to 17.7 and the correlation became stronger (R^2 = 0.98). This shift occurred between 8 and 24 h into the experiment, as Fe dissolution transitioned from the early, fast stage to the late, slower stage (**Figures 3D**, **4A**). The Al-to-Fe and Si-to-Al correlations could only be established for the late stage, in which the slopes were 4.6 (R^2 = 0.96; **Figure 5B**) and 2.9 (R^2 = 0.96, **Supplementary Figure S1**), respectively. Al concentration data in the early stage was too noisy to be considered in this analysis.

From the strong correlation between Fe, Si, and Al concentrations in the late SD stage, we hypothesize that these elements were solubilized from a mutual mineral source and that this mineral, or mineral group, was the dominant Fe source after the initial 24 h.

Temperature Effect

To further investigate the nature of the two-stage Fe dissolution observed with the siderophore, we repeated the experiment at different temperatures (7–50°C; **Figure 6**). The rates of SD of Fe, Al, and Si were strongly affected by the suspension temperature (**Figure 6A** and **Supplementary Figure S2**), yet the correlations between the dissolved concentrations remained consistent and strong ($S_{Si/Fe}$ = 15.1, R^2 = 0.97; $S_{Al/Fe}$ = 3.6, R^2 = 0.93; **Figure 6B**), giving further indication for a common source. Based on the hypothesis that the fast initial Fe mobilization is due to a siderophore-controlled Fe(hydr)oxides dissolution mechanism and the assumption that the adsorbed siderophore concentration is not strongly affected by temperature (Walter et al., 2017), we can assume that constructing an Arrhenius plot of the natural logarithm of the rate, rather than the rate coefficient, will neither affect the slope nor the calculated activation energy (**Figure 6C**). Noting that the data follows a linear trend, we calculated an apparent activation energy of 32.4 kJ/mol. This is in close agreement with an apparent activation energy observed previously for DFOB-promoted dissolution of goethite of 28.5 kJ/mol (Cocozza et al., 2002). Unfortunately, we could not discern steady-state dissolution for the subsequent slow dissolution phase. Therefore, no attempt was made to construct an Arrhenius plot for this phase.

All the original data is found in the **Supplementary Material**.

DISCUSSION

Conceptual Dust Dissolution Model

In an effort to characterize dust-Fe dissolution in *Trichodesmium* colonies, we measured dust dissolution in seawater by two biological dissolution mechanisms: dissolution in the presence of a siderophore and a reductant. Examining the concentrations of the dissolved elements Fe, Al, and Si in all dissolution experiments we identified two release stages: (1) initial fast Fe dissolution at low Si/Fe ratios and (2) subsequent dissolution of Fe, Si, and Al at a constant stoichiometry and a high Si/Fe ratio. We postulate that the first stage involves dissolution of a mineral that contains mostly Fe, most likely Fe(hydr)oxides, and that the second stage represents dissolution of minerals that contain Fe, Al, and Si, most likely Fe-bearing aluminosilicates. To clarify and integrate our findings and interpretations, we graphically summarize them in a conceptual dissolution model, which is presented in **Figure 7**.

A RD pathway with ascorbate as a reductant is addressed in **Figure 7A**. We observed that increasing ascorbate concentrations only increased the release of Fe, but not of Si or Al (**Figures 3**, **4**), except for the highest ascorbate concentration, presumably due to the formation of Al-ascorbate complexes. This suggests that Fe(hydr)oxides were the primary dissolving mineral throughout the experiment. Si release in the presence of ascorbate was similar to the ascorbate-free control, indicating that ascorbate did not induce dissolution of aluminosilicates (**Figure 4D**). However, the baseline dissolution of aluminosilicates may still contribute some dissolved Fe in these experiments. Based on Si accumulation in solution and the Si:Fe ratios obtained in SD, we estimate that the amount of Fe released from aluminosilicates [assuming that it remains in solution as reduced Fe(II)] accounts for 15–40% of the released Fe, depending on ascorbate concentration. It should be noted, that at the largest ascorbate concentration (300 μM), dissolution of Al and Si was slightly increased in the late stage (**Figure 4D**), suggesting that under these conditions a small fraction of the Fe dissolved was also contributed by RD of aluminosilicates. Enhanced Si dissolution at high ascorbate concentrations has been previously reported with quartz and crocidolite, but

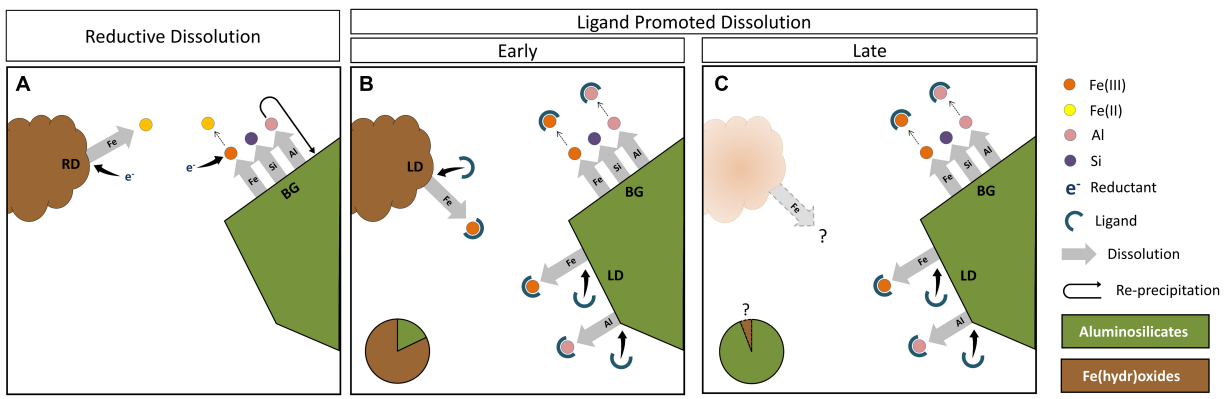

FIGURE 7 | A schematic representation of the major dissolution pathways and principal minerals contributing to the release of Fe, along with Al and Si, into seawater from dust, via two mechanisms employed by phytoplankton. The presence of a reductant **(A)** enhances the dissolution rate of Fe(hydr)oxides (RD), but not that of aluminosilicates, which dissolve at a background rate (BG). Dissolved Fe is maintained in solution in its reduced and more soluble form, Fe(II). The presence of the siderophore **(B,C)** enhanced the dissolution of both Fe(hydr)oxides and aluminosilicates (SD). Complexation of both Fe and Al by the siderophore prevent their precipitation as (hydr)oxides and allows accumulation in solution. In early SD **(B)**, Fe release was poorly correlated to Si and Al release, indicating that Fe(hydr)oxides were the main dissolving Fe pool. In contrast, in late SD **(C)**, Fe release was strongly correlated to Al and Si release, indicating that Fe-bearing aluminosilicates were the main dissolving Fe pool. The relative contribution of the different Fe-pools in the presence of a siderophore is depicted in the pie-charts in **B,C**. The pie piece with the question mark represents a small, unquantified contribution from another Fe pool.

the mechanism has not been clarified (Fenoglio et al., 2000; Martra et al., 2003).

Figures 7B,C show the mechanisms of Fe release by SD, where the dissolution pattern shifted over time from low to high Si/Fe ratio (**Figures 3–5**). This pattern suggests that at early SD, Fe(hydr)oxides contributed most of the Fe (**Figure 7B**), while at late SD, aluminosilicates became the dominant Fe source (**Figure 7C**). Siderophore-controlled dissolution of Fe(hydr)oxides in the early stage is also consistent with the temperature dependence patterns (**Figure 6C**) that indicate a similar activation energy as previously observed in DFOB-promoted dissolution of Fe(hydr)oxides, as discussed above. Assuming constant Fe release from aluminosilicates throughout the experiment, we estimate that Fe(hydr)oxides contributed 80% of the released Fe in the early stage, and aluminosilicates only 20% (as depicted in the pie-chart in **Figure 7B**). While we have evidence that the majority of Fe released in the late stage originated from aluminosilicates, there still might be some residual contribution of Fe(hydr)oxides. From the shift between the dissolution stages, we can estimate the proportion of the most readily dissolvable Fe(hydr)oxides in the sample to be ∼0.5 μM Fe (i.e., 1.7 μmol Fe g^{-1} $Dust^{-1}$ d^{-1}) or ∼0.3% of the dust-Fe. Dissolution of Fe, Al, and Si were greatly accelerated by the presence of the siderophore, as indicated by the effect of DFOB on dissolution rates (**Figure 4**). We hypothesize that the DFOB attack on Fe and Al surface sites created more reactive Si surface sites and indirectly accelerated Si dissolution. The coupling of SD of Al and Fe to enhanced Si dissolution has been previously demonstrated for several silicates commonly found in desert dust (Wieland and Stumm, 1992; Liermann et al., 2000; Rosenberg and Maurice, 2003; Walter et al., 2019).

Interpreting our dissolution data through the scope of our conceptual model, we conclude that under certain conditions aluminosilicates contributed more to Fe dissolution than Fe(hydr)oxides. Examining the composition of aluminosilicates in our dust sample, we observe that the most dominant fraction is composed of small (2.5 ± 1 μM) clay and mica particles, with a large surface area and detectable Fe levels (**Table 1** and **Figure 2**). The Fe content in the other aluminosilicates, albite, and actinolite, was too low to be detected by EDS (**Supplementary Figure S3**), suggesting that they are not major contributors to the total Dust-Fe. For these reasons we suggest that clays are the source of silica-associated Fe that was released by SD. Furthermore, we find that the dissolved Si-to-Al ratios (2.9; **Supplementary Figure S1**) are similar to Si-to-Al ratios in the clays (2.6; **Figure 2C**), suggesting that congruent dissolution of this mineral group contributed a significant portion of the dissolved Al and Si. Since the measured Fe content of the clay aggregates (**Figure 2C**) was probably influenced by small Fe(hydr)oxides particles, the ratios of Si- and Al-to-Fe, in the solid and the dissolved, are not comparable.

Dust-Fe Dissolution Patterns

Bi-modal dissolution of dust-Fe has been previously observed directly in seawater of the Mediterranean, which naturally contained ∼2.5 nM of Fe-binding ligands (Wagener et al., 2008). Similar to our observed dissolution pattern, dust-Fe dissolution in Mediterranean seawater was initially fast but quickly dropped by approximately twofold. Similar dust-Fe dissolution patterns were also observed in simulated atmospheric processing of Sahara dust at low pH (Shi et al., 2011); in this study, the authors assumed clay-minerals, such as illite, to be the source of the slow dissolving Fe in the late stage. Together, these observations imply that bi-modal dust-Fe dissolution is ubiquitous in dust-Fe dissolution.

The total amount of Fe that was extracted from dust in our experiment was found to be comparable to extraction procedures, which have been used in the past to experimentally determine the percentage of soluble Fe in desert-dust. These procedures used different leaching solutions, dust concentrations and physical setups, and in turn yielded a large range of solubility estimates, from **0.04** to **5%** (Aguilar-Islas et al., 2010). These solubility estimates are potentially relevant for different dissolution scenarios, from immediate Fe release upon deposition to prolonged remineralization processes. In this study, we identified the fraction of fast dissolving Fe (8 h) to be **0.3%** of the dust-Fe, within the range of previously reported percent solubilities. We cannot determine the size of the slow dissolving Fe pool, since it was not depleted in the course of our experiment; however, we can say it was at least **2.7%** of the dust mass (based on the highest dissolved Fe concentration measured at 50°C; **Figure 6A**).

In contrast to our expectations, the fraction of fast dissolving Fe(hydr)oxides (0.3%) was small in comparison to the amorphous Fe fraction, as operationally defined by the ammonium oxalate extraction: 5%. This suggests that a large fraction of the amorphous Fe(hydr)oxide minerals that were detected in the oxalate extract were too stable for fast SD by DFOB, under the experimental conditions. In contrast to stable Fe(hydr)oxides, in which Fe is tightly bound to oxygen atoms, in aluminosilicates Fe is found as a substitution for Al in octahedral sites or for potassium in the inter-sheets structure (Johnston and Cardile, 1987). Our model suggests that clay-Fe may be more susceptible to LD by DFOB than stable Fe(hydr)oxides.

Clays – A Dominant Factor in SD of Dust-Fe

Clays are one of the main constituents of desert dust, accounting for 40–80% of the dust mass (**Table 1**; Glaccum and Prospero, 1980; Avila et al., 1997; Journet et al., 2008). Due to their small size, dust-clay particles reach remote open waters (Gao et al., 2003; Jeong, 2008; Jeong and Achterberg, 2014) and have a long residence time in the photic zone (100–200 days; Deuser et al., 1983; Jickells et al., 1990). Clay minerals contain less Fe than Fe(hydr)oxides: 0–22 wt% (Stucki et al., 2012), but since clays are often significantly more abundant in dust than Fe(hydr)oxides, clay-Fe may be the largest pool in dust (Journet et al., 2008). A key finding of this study is the important role of clays in SD release of Fe from dust. After 24 h, when the most

readily available Fe(hydr)oxide pool became exhausted, the siderophore induced significant release of dissolved Fe from clays, which lasted throughout the 8-day incubation. This finding is in-line with several recent studies, which also found clays to be a major source of Fe to the oceans, in different dissolution setups: atmospheric processing simulations (Cwiertny et al., 2008; Shi et al., 2011; Paris and Desboeufs, 2013), fractional solubility studies (Journet et al., 2008; Schroth et al., 2009) and in phytoplankton growth experiments (Shoenfelt et al., 2017). Our experiments reveal that clays are also susceptible to siderophore-promoted dissolution in seawater, further establishing them as an important source of Fe in the marine environment.

In the Gulf of Aqaba clays are frequently observed in the core of *Trichodesmium* colonies, as in the colony shown in **Figure 1A**. In light of our findings we speculate that *Trichodesmium* can not only benefit from labile iron oxides, but also take advantage from more slowly dissolving clays over longer timescales. In addition to supporting its own growth, dust processing by *Trichodesmium* may also supply its surrounding with a flux of dissolved nutrients and impact the overall productivity of the ecosystem. Here, we observed that the dissolution of clays by the siderophore also released significant amount of Si into solution. For diatoms communities in the Equatorial Pacific and Southern Ocean, which have been shown to be co-limited by Fe and Si (Brzezinski et al., 2011; Hoffmann et al., 2007), the coupling between enhanced Fe and Si dissolution may have important biogeochemical implications.

Apart from being an Fe source, our data indicate that clays in dust are also a significant sink for free siderophore ligands through complexation of dissolving competing metals such as Al. This competitive effect was observed at the lowest applied concentration of siderophore (3 μM DFOB; **Figures 3**, **4**), when most DFOB was bound to Al after 24 h, completely repressing further SD of Fe (see section "Siderophore-Promoted Dissolution"). Siderophores, such as ferrioxamines, are known to bind several metals other than Fe, especially Al (Martell and Smith, 1975; Schenkeveld et al., 2016). Hence, under certain conditions, when unbound siderophore concentrations are the limiting factor for dissolution, the presence of clays may inhibit Fe dissolution.

Implications to *Trichodesmium*'s Fe Requirements

Going back to natural *Trichodesmium* colonies that collect and concentrate dust particles in their cores, we can apply the measured SD rates to assess the supply of dissolved Fe to *Trichodesmium* from dust. Using the range of observed dust masses collected by single colonies of 0.03–0.3 μg (see section "Estimation of Dust Loads on *Trichodesmium* Colonies") and the late SD release rates of 2 and 0.4 μmol Fe g^{-1} $Dust^{-1}$ d^{-1}, we calculated Fe supply rates that vary from 0.01 to 0.6 pmol Fe $colony^{-1}$ d^{-1} (**Figure 8A** and **Supplementary Table S2**). Based on a recent report by Basu et al. (2019) of enhanced Fe uptake rates in the presence of DFOB, we assume that the Fe released by SD is bioavailable to *Trichodesmium*. Hence, we can compare the Fe supply rates with the colony's Fe requirements, calculated by multiplying the colony's Fe quota by its growth rate. Both colony Fe quota and growth rate depend on Fe and phosphorus availability, as well as on other environmental variables (Chappell et al., 2012). We hence chose a range of published values (**Supplementary Table S2**) and obtained Fe requirements that range from a minimum of 0.3 pmol Fe $colony^{-1}$ d^{-1} to a maximum of 60 pmol Fe $colony^{-1}$ d^{-1} (**Supplementary Table S1** and **Figure 8B**). This broad range covers scenarios from growth under severe Fe limitation, at a very slow rate (0.01 d^{-1}) and low Fe quotas $\left(30\ \text{pmol Fe colony}^{-1}\text{d}^{-1}\right)$, to Fe replete growth, at a fast rate (0.15 d^{-1}) and a high Fe quota

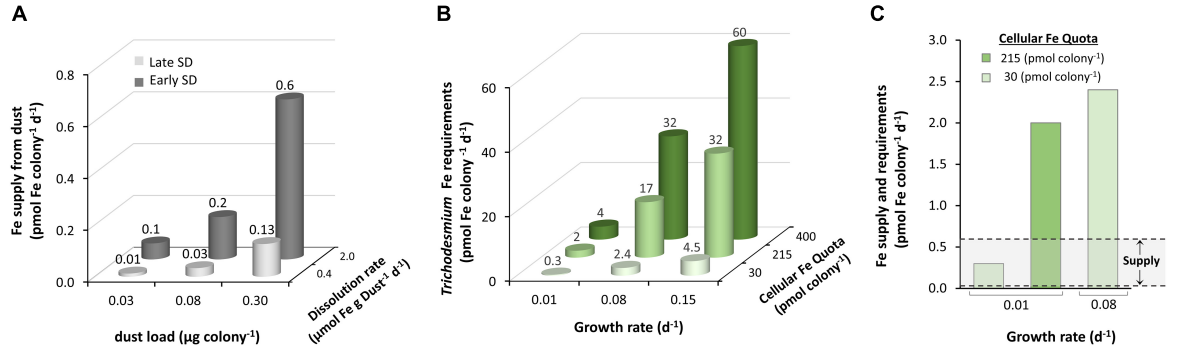

FIGURE 8 | *Trichodesmium's* Fe demand versus Fe supply from dust. **(A)** The supply of dissolved Fe from dust particles, associated with *Trichodesmium* colonies, was calculated for the range of observed dust loads (see section "Estimation of Dust Loads on *Trichodesmium* Colonies"), combined with dissolution rates measured in late and early SD, with 9 μM and 3 μM DFOB, respectively. **(B)** Fe demand of *Trichodesmium* colonies was calculated for a range of cellular Fe quotas and growth rates, reported in the literature (more details in **Supplementary Table S1**). **(C)** Comparing the lower end of Fe demands that are suitable for Fe-limited *Trichodesmium* (green bars; 0.3 – 2.4 pmol Fe $colony^{-1}$ d^{-1}) to the range of Fe supply from dust (gray zone; 0.01–0.6 pmol Fe $colony^{-1}$ d^{-1}) demonstrates that dust can fully supply the demand of only the slowest growing, most Fe limited colonies. In other scenarios, the estimated Fe supply only meets a fraction of the demand.

$(400\ \text{pmol Fe colony}^{-1}\text{d}^{-1})$. In the lower range ($0.3 - 2.4$ pmol Fe colony^{-1} d^{-1}), Fe release from dust exceeds the minimal daily requirements (200% supply-to-requirement), but only supplies 30% of the requirements at the top of this range (**Figure 8C**). For colonies with high Fe requirements ($17 - 60$ pmol Fe colony^{-1} d^{-1}), dust can supply only a negligible fraction of the required Fe (1–3%). These calculations imply that in many cases colonies require additional Fe sources in order to grow or are able to utilize dust-Fe more efficiently than estimated here.

Indeed, many additional factors may play a role in dust-Fe dissolution within *Trichodesmium* colonies. Unlike our dark-conducted incubations, dust particles within *Trichodesmium* are exposed to fluctuating light intensities over the day–night cycle. Photo-dissolution of Fe(hydr)oxides, which is considered negligible at pH 8 (Waite and Morel, 1984), has been shown to accelerate in the presence of DFOB (Borer et al., 2005) and thus can potentially enhance dust-Fe SD during the day. Furthermore, dissolved Fe(II), released by biologic reduction, may have a longer life-time within the colony microenvironment than in solution, due to photochemical processes and to the fact that the pH and oxygen levels within *Trichodesmium* colony decrease during the night (Eichner et al., 2019a,b). Furthermore, Gledhill et al. (2019) have shown that *Trichodesmium* colonies from the Gulf of Aqaba secrete a mixture of 18 Fe-binding metallophores. The simultaneous activity of different siderophores, combined with the colony's reducing power, may act synergistically and result in faster dissolution of dust-Fe. *Trichodesmium* may also optimize its Fe supply from particles by selective collection of particles that contain Fe. We recently demonstrated that natural *Trichodesmium* colonies can distinguish between Fe-rich and Fe-free particles and are capable of selective collection and retention of Fe-rich particles in their cores (Kessler et al., 2019). Further research is required to unfold the pathways employed by *Trichodesmium* to mine valuable nutrients such as Fe and probably *P* from dust. These pathways assist *Trichodesmium* in establishing large surface blooms in vast nutrient-poor ocean regions and fuel primary and secondary productivity with fixed nitrogen and carbon and possibly even dissolved Fe that originated from dust or other particles.

DATA AVAILABILITY STATEMENT

All datasets generated for this study are included in the article/**Supplementary Material**.

AUTHOR CONTRIBUTIONS

NK designed and conducted the experiments, analyzed the data, and wrote the manuscript. YS assisted in experiment design, data analysis, manuscript preparation, and contributed from her expertise in marine biogeochemistry. SK assisted and supervised in the experiment design, data analysis, manuscript preparation, and contributed from his expertise in environmental geochemistry. WS designed the experiments and assisted in their conduction, took part in the data analysis, and manuscript preparation.

FUNDING

YS and her group were partly supported by the Israel Science Foundation grant 458/15 (www.isf.org.il) and the German-Israeli Foundation for Scientific Research and Development grant #1349 (www.GIF.org.il). Funding for SK and WS was provided by the Austrian FWF (I2865-N34). Research visit of NK at UV was supported by an Alfred Ebenbauer scholarship granted by the University of Vienna.

ACKNOWLEDGMENTS

We thank Dr. Martin Walter for his help with the ICP-OES measurements and Prof. Nir Keren for his guidance and support.

SUPPLEMENTARY MATERIAL

The Supplementary Material for this article can be found online at: https://www.frontiersin.org/articles/10.3389/fmars.2020.00045/full#supplementary-material

REFERENCES

Aguilar-Islas, A. M., Wu, J., Rember, R., Johansen, A. M., and Shank, L. M. (2010). Dissolution of aerosol-derived iron in seawater: leach solution chemistry, aerosol type, and colloidal iron fraction. *Mar. Chem.* 120, 25–33. doi: 10.1016/j.marchem.2009.01.011

Avila, A., Queralt-Mitjan, I., and Alarcon, M. (1997). Mineralogical composition of African dust delivered by red rains over northeastern Spain. *J. Geophys. Res.* 102, 977–996.

Basu, S., Gledhill, M., de Beer, D., Prabhu Matondkar, S. G., and Shaked, Y. (2019). Colonies of marine cyanobacteria Trichodesmium interact with associated bacteria to acquire iron from dust. *Commun. Biol.* 2, 1–8. doi: 10.1038/s42003-019-0534-z

Basu, S., and Shaked, Y. (2018). Mineral iron utilization by natural and cultured Trichodesmium and associated bacteria. *Limnol. Oceanogr.* 63, 2307–2320. doi: 10.1002/lno.10939

Berman-Frank, I., Cullen, J. T., Shaked, Y., Sherrell, R. M., and Falkowski, G. (2001). Iron availability, cellular iron quotas, and nitrogen fixation in Trichodesmium. *Limnol. Oceanogr.* 46, 1249–1260. doi: 10.4319/lo.2001.46.6.1249

Bif, M. B., and Yunes, J. S. (2017). Distribution of the marine cyanobacteria Trichodesmium and their association with iron-rich particles in the South Atlantic Ocean. *Aquat. Microb. Ecol.* 78, 107–119. doi: 10.3354/ame01810

Bligh, M. W., and Waite, T. D. (2011). Formation, reactivity, and aging of ferric oxide particles formed from Fe(II) and Fe(III) sources: implications for iron bioavailability in the marine environment. *Geochi.Cosmoch. Acta* 75, 7741–7758. doi: 10.1016/j.gca.2011.10.013

Boiteau, R. M., Mende, D. R., Hawco, N. J., McIlvin, M. R., Fitzsimmons, J. N., Saito, M. A., et al. (2016). Siderophore-based microbial adaptations to iron scarcity across the eastern Pacific Ocean. *Proc. Natl.Acad. Sci. U.S.A* 113, 14237–14242. doi: 10.1073/pnas.1608594113

Borer, P. M., Sulzberger, B., Reichard, P., and Kraemer, S. M. (2005). Effect of siderophores on the light-induced dissolution of colloidal iron(III) (hydr)oxides. *Mar. Chem.* 93, 179–193. doi: 10.1016/j.marchem.2004.08.006

Boyd, P. W., Mackie, D. S., and Hunter, K. A. (2010). Aerosol iron deposition to the surface ocean - Modes of iron supply and biological responses. *Mar. Chem.* 120, 128–143. doi: 10.1016/j.marchem.2009.01.008

Brzezinski, M. A., Baines, S. B., Balch, W. M., Beucher, C. P., Chai, F., Dugdale, R. C., et al. (2011). Co-limitation of diatoms by iron and silicic acid in the equatorial Pacific Deep-Sea Research II. *Deep Sea Res. Part II* 58, 493–511. doi: 10.1016/j.dsr2.2010.08.005

Byrne, R. H., and Kester, D. R. (1976). Solubility of hydrous ferric oxide and iron speciation in seawater. *Mar. Chem.* 4, 255–274. doi: 10.1016/0304-4203(76)90012-8

Carpenter, E. J., Capone, D. G., and Rueter, J. G. (1992). *Marine Pelagic Cyanobacteria. Trichodesmium and Other Diazotrophs*. Berlin: Springer Science & Business Media.

Chappell, P. D., Moffett, J. W., Hynes, A. M., and Webb, E. A. (2012). Molecular evidence of iron limitation and availability in the global diazotroph Trichodesmium. *ISME J.* 6, 1728–1739. doi: 10.1038/ismej.2012.13

Chen, Y., Mills, S., Street, J., Golan, D., Post, A., Jacobson, M., et al. (2007). Estimates of atmospheric dry deposition and associated input of nutrients to Gulf of Aqaba seawater. *J. Geophys. Res. Atmos.* 112, 1–14.

Chen, Y., Paytan, A., Chase, Z., Measures, C., Beck, A. J., Sañudo-Wilhelmy, S. A., et al. (2008). Sources and fluxes of atmospheric trace elements to the Gulf of Aqaba. Red Sea. *J. Geophys. Res. Atmos.* 113, 1–13. doi: 10.1016/j.marpolbul.2014.11.047

Cocozza, C., Tsao, C. C. G., Cheah, S. F., Kraemer, S. M., Raymond, K. N., Miano, T. M., et al. (2002). Temperature dependence of goethite dissolution promoted by trihydroxamate siderophores. *Geochim. Cosmochim. Acta* 66, 431–438. doi: 10.1016/s0016-7037(01)00780-3

Conway, T. M., and John, S. G. (2014). Quantification of dissolved iron sources to the North Atlantic Ocean. *Nature* 511, 212–215. doi: 10.1038/nature13482

Croot, P. L., and Johansson, M. (2000). Determination of iron speciation by cathodic stripping voltammetry in seawater using the competing ligand 2-(2-thiazolylazo)-p-cresol (TAC). *Electroanalysis* 12, 565–576. doi: 10.1002/(sici)1521-4109(200005)12:8<565::aid-elan565>3.0.co;2-l

Cwiertny, D. M., Baltrusaitis, J., Hunter, G. J., Laskin, A., Scherer, M. M., and Grassian, V. H. (2008). Characterization and acid-mobilization study of iron-containing mineral dust source materials. *J. Geophys.Res. Atmos.* 113, 1–18. doi: 10.1016/j.jes.2018.04.012

Deuser, W. G., Brewer, P. G., Jickells, T. D., and Commeau, R. F. (1983). Biological control of the removal of abiogenic particles from the surface ocean. *Science* 219, 388–391. doi: 10.1126/science.219.4583.388

Duce, R. A., and Tindale, N. W. (1991). Atmospheric transport of iron and its deposition in the ocean. *Limnol. Oceanogr.* 36, 1715–1726. doi: 10.4319/lo.1991.36.8.1715

Eichner, M., Basu, S., Gledhill, M., de Beer, D., and Shaked, Y. (2019a). Hydrogen dynamics in trichodesmium colonies and their potential role in mineral iron acquisition. *Front. Microbiol.* 10:1565. doi: 10.3389/fmicb.2019.01565

Eichner, M., Basu, S., Wang, S., de Beer, D., and Shaked, Y. (2019b). Mineral iron dissolution in Trichodesmium colonies. The role of O2 and pH microenvironments. *Limnol. Oceanogr.* 2019, 1–12.

Fenoglio, I., Martra, G., Coluccia, S., and Fubini, B. (2000). Possible role of ascorbic acid in the oxidative damage induced by inhaled crystalline silica particles. *Chem. Res. Toxicol.* 13, 971–975. doi: 10.1021/tx000125h

Frischkorn, K. R., Rouco, M., Van Mooy, B. A. S., and Dyhrman, S. T. (2017). Epibionts dominate metabolic functional potential of Trichodesmium colonies from the oligotrophic ocean. *ISME J.* 11, 2090–2101. doi: 10.1038/ismej.2017.74

Ganor, E., Foner, H. A., Brenner, S., Neeman, E., and Lavi, N. (1991). The chemical composition of aerosols settling in Israel following dust storms. *Atmos. Environ. Part A Gen. Top.* 25, 2665–2670. doi: 10.1016/0960-1686(91)90196-e

Gao, Y., Fan, S.-M., and Sarmiento, J. L. (2003). Aeolian iron input to the ocean through precipitation scavenging: a modeling perspective and its implication for natural iron fertilization in the ocean. *J Geophys. Res.* 108:4221.

Glaccum, R. A., and Prospero, J. M. (1980). Saharan aerosols over the tropical North Atlantic-Mineralogy. *Mar. Geol.* 37, 295–321. doi: 10.1016/0025-3227(80)90107-3

Gledhill, M., Basu, S., and Shaked, Y. (2019). Metallophores associated with Trichodesmium erythraeum colonies from the Gulf of Aqaba. *Metallomics* 11, 1547–1557. doi: 10.1039/c9mt00121b

Granger, J., and Price, N. M. (1999). The Importance of siderophores in iron nutrition ofheterotrophic marine bacteria. *Limnol. Oceanogr.* 44, 541–555. doi: 10.4319/lo.1999.44.3.0541

Hernandez, M. E. (2001). Extracellular electron transfer. *Cell. Mol.life Sci.* 58, 1562–1571.

Hoffmann, L. J., Peeken, I., and Lochte, K. (2007). Co-limitation by iron, silicate, and light of three Southern Ocean diatom species. *Biogeosci. Discuss.* 4, 209–247. doi: 10.5194/bgd-4-209-2007

Hyacinthe, C., Bonneville, S., and Van Cappellen, P. (2006). Reactive iron(III) in sediments: chemical versus microbial extractions. *Geochim. Cosmochim. Acta* 70, 4166–4180. doi: 10.1016/j.gca.2006.05.018

Jeong, G. Y. (2008). Bulk and single-particle mineralogy of Asian dust and a comparison with its source soils. *J. Geophys. Res. Atmos.* 113, 1–16.

Jeong, G. Y., and Achterberg, E. P. (2014). Chemistry and mineralogy of clay minerals in Asian and Saharan dusts and the implications for iron supply to the oceans. *Atmos. Chem. Phys.* 14, 12415–12428. doi: 10.5194/acp-14-12415-2014

Jickells, T. D., An, Z. S., Andersen, K. K., Baker, A. R., Bergametti, G., Brooks, N., et al. (2005). Global iron connections between desert dust, ocean biogeochemistry, and climate. *Science* 308, 67–71. doi: 10.1126/science.1105959

Jickells, T. D., Deuser, W. G., and Belastock, R. A. (1990). Temporal variations in the concentrations of some particulate elements in the surface waters of the Sargasso Sea and their relationship to deep-sea fluxes. *Mar.Chem.* 29, 203–219. doi: 10.1016/0304-4203(90)90014-4

Johnston, J. H., and Cardile, C. M. (1987). Iron Substitution in montmorillonite, illite, and glauconite by 57Fe mössbauer spectroscopy. *Clays Clay Minerals* 35, 170–176. doi: 10.1346/ccmn.1987.0350302

Jolivet, J. P., Chanéac, C., and Tronc, E. (2004). Iron oxide chemistry. From molecular clusters to extended solid networks. *Chem. Commun.* 481–483. doi: 10.1039/b304532n

Journet, E., Desboeufs, K. V., Caquineau, S., and Colin, J. L. (2008). Mineralogy as a critical factor of dust iron solubility. *Geophys. Res.Lett.* 35, 3–7.

Kessler, N., Armoza-Zvuloni, R., Wang, S., Basu, S., Weber, P. K., Stuart, R. K., et al. (2019). Selective collection of iron-rich dust particles by natural Trichodesmium colonies. *ISME J.* 14, 91–103. doi: 10.1038/s41396-019-0505-x

Kraemer, S. M., Butler, A., and Borer, P. (2005). Siderophores and the dissolution of iron-bearing minerals in marine systems. *Rev. Mineral. Geochem.* 59, 53–84. doi: 10.2138/rmg.2005.59.4

Kraemer, S. M., Duckworth, O. W., Harrington, J. M., and Schenkeveld, W. D. C. (2015). Metallophores and trace metal biogeochemistry. *Aquat Geochem.* 21, 159–195. doi: 10.1007/s10498-014-9246-7

Kranzler, C., Kessler, N., Keren, N., and Shaked, Y. (2016). Enhanced ferrihydrite dissolution by a unicellular, planktonic cyanobacterium: a biological contribution to particulate iron bioavailability. *Environ. Microbiol.* 18, 5101–5111. doi: 10.1111/1462-2920.13496

Kuhn, K. M., DuBois, J. L., and Maurice, P. A. (2013). Strategies of aerobic microbial Fe acquisition from Fe-bearing montmorillonite clay. *Geochim. Cosmochim. Acta* 117, 191–202. doi: 10.1016/j.gca.2013.04.028

Kuma, K., and Matsunaga, K. (1995). Availability of colloidal ferric oxides to coastal marine phytoplankton. *Mar. Biol.* 122, 1–11. doi: 10.1007/bf00349272

Kuma, K., Nishioka, J., and Matsunaga, K. (1996). Controls on iron(III) hydroxide solubility in seawater: the influence of pH and natural organic chelators. *Limnol. Oceanogr.* 41, 396–407. doi: 10.4319/lo.1996.41.3.0396

Kustka, A., Sañudo-Wilhelmy, S., Carpenter, E. J., Capone, D. G., and Raven, J. A. (2003). A revised estimate of the iron use efficiency of nitrogen fixation, with special reference to the marine cyanobacterium Trichodesmium spp.(Cyanophyta) 1. *J. Phycol.* 39, 12–25. doi: 10.1046/j.1529-8817.2003.01156.x

Langlois, R. J., Mills, M. M., Ridame, C., Croot, P., and LaRoche, J. (2012). Diazotrophic bacteria respond to Saharan dust additions. *Mar. Ecol. Progr. ss Ser.* 470, 1–14. doi: 10.3354/meps10109

Liermann, L. J., Kalinowski, B. E., Brantley, S. L., and Ferry, J. G. (2000). Role of bacterial siderophores in dissolution of hornblende. *Geochim. Cosmochim. Acta* 64, 587–602. doi: 10.1016/s0016-7037(99)00288-4

Lis, H., Kranzler, C., Keren, N., and Shaked, Y. (2015). A comparative study of iron uptake rates and mechanisms amongst marine and fresh water cyanobacteria: prevalence of reductive iron uptake. *Life* 5, 841–860. doi: 10.3390/life5010841

Liu, X., and Millero, F. J. (2002). The solubility of iron in seawater. *Mar. Chem.* 77, 43–54. doi: 10.1016/s0304-4203(01)00074-3

Maldonado, M. T., Strzepek, R. F., Sander, S., and Boyd, P. W. (2005). Acquisition of iron bound to strong organic complexes, with different Fe binding groups and photochemical reactivities, by plankton communities in Fe-limited subantarctic waters. *Global Biogeochem. Cycles* 19:GB4S23.

Martell, A. E., and Smith, R. M. (1975). *Critical Stability Constants*, Vol. 5. New York, NY: Plenum Press, 301–305.

Martin, J. H., Gordon, M., and Fitzwater, S. E. (1991). The case for iron. *Limnol. Oceanogr.* 36, 1793–1802. doi: 10.4319/lo.1991.36.8.1793

Martra, G., Tomatis, M., Fenoglio, I., Coluccia, S., and Fubini, B. (2003). Ascorbic acid modifies the surface of asbestos. possible implications in the molecular mechanisms of toxicity. *Chem. Res. Toxicol.* 16, 328–335. doi: 10.1021/tx0200515

Moore, C. M., Mills, M. M., Arrigo, K. R., Berman-Frank, I., Bopp, L., Boyd, P. W., et al. (2013). Processes and patterns of oceanic nutrient limitation. *Nat. Geosci.* 6, 701–710. doi: 10.1038/ngeo1765

Morel, F. M. M., and Price, N. M. (2003). The biogeochemical cycles of trace metals in the oceans. *Science* 300, 944–947. doi: 10.1126/science.1083545

Morel, F. M. M., Rueter, J. G., Anderson, D. M., and Guillard, R. R. L. (1979). Aquil: a chemically defined phytoplankton culture medium for trace metal studies. *J. Phycol.* 15, 135–141. doi: 10.1007/s10534-019-00215-2

Nodwell, L. M., and Price, N. M. (2001). Direct use of inorganic colloidal iron by marine mixotrophic phytoplankton. *Limnol. Oceanogr.* 46, 765–777. doi: 10.4319/lo.2001.46.4.0765

Nuester, J., Vogt, S., Newville, M., Kustka, A. B., and Twining, B. S. (2012). The unique biogeochemical signature of the marine diazotroph Trichodesmium. *Front. Microbiol.* 3:159. doi: 10.3389/fmicb.2012.00150

Paris, R., and Desboeufs, K. V. (2013). Effect of atmospheric organic complexation on iron-bearing dust solubility. *Atmos. Chem. Phys.* 13, 4895–4905. doi: 10.5194/acp-13-4895-2013

Partridge, N. A., Regnier, F. E., White, J. L., and Hem, S. L. (1989). Influence of dietary constituents on intestinal absorption of aluminum. *Kidney Int.* 35, 1413–1417. doi: 10.1038/ki.1989.142

Polyviou, D., Baylay, A. J., Hitchcock, A., Robidart, J., Moore, C. M., and Bibby, T. S. (2018). Desert dust as a source of iron to the globally important diazotroph Trichodesmium. *Front. Microbiol.* 8:2683. doi: 10.3389/fmicb.2017.02683

Roe, K. L., and Barbeau, K. (2014). Uptake mechanisms for inorganic iron and ferric citrate in Trichodesmium erythraeum IMS101: metallomics. *Integr. .Biometal Sci.* 6, 2042–2051. doi: 10.1039/c4mt00026a

Rosenberg, D. R., and Maurice, P. A. (2003). Siderophore adsorption to and dissolution of kaolinite at pH 3 to 7 and 22°C. *Geochim. Cosmochim. Acta* 67, 223–229. doi: 10.1016/s0016-7037(02)01082-7

Rubin, M., Berman-Frank, I., and Shaked, Y. (2011). Dust- and mineral-iron utilization by the marine dinitrogen-fixer Trichodesmium. *Nat. Geosci.* 4, 529–534. doi: 10.1038/ngeo1181

Rue, E. L., and Bruland, K. W. (1995). Complexation of iron(III) by natural organic ligands in the Central North Pacific as determined by a new competitive ligand equilibration/adsorptive cathodic stripping voltammetric method. *Mar. Chem.* 50, 117–138. doi: 10.1016/0304-4203(95)00031-l

Rueter, J. G., Hutchins, D. A., Smith, R. W., and Unsworth, N. L. (1992). "Iron Nutrition in Trichodesmium," in *Marine Pelagic Cyanobacteria: Trichodesmium and Other Diazotrophs*, eds E. J. Carpenter, D. G. Capone, and J. G. Rueter (South Holland: Kluwer Academic), 289–306. doi: 10.1007/978-94-015-7977-3_19

Schenkeveld, W. D. C., Wang, Z., Giammar, D. E., and Kraemer, S. M. (2016). Synergistic E ff ects between Biogenic Ligands and a Reductant in Fe Acquisition from Calcareous Soil. *Environ. Sci. Technol.* 50, 6381–6388. doi: 10.1021/acs.est.6b01623

Schroth, A. W., Crusius, J., Sholkovitz, E. R., and Bostick, B. C. (2009). Iron solubility driven by speciation in dust sources to the ocean. *Nat. Geosci.* 2, 337–340. doi: 10.1038/ngeo501

Schwertmann, U. (1964). The differentiation of iron oxides in soil by extraction with ammonium-oxalate solution. *J. Plant Nutr.Soil Sci.* 105, 194–202.

Shi, Z., Bonneville, S., Krom, M. D., Carslaw, K. S., Jickells, T. D., Baker, A. R., et al. (2011). Iron dissolution kinetics of mineral dust at low pH during simulated atmospheric processing. *Atmos. Chem. Phys.* 11, 995–1007. doi: 10.5194/acp-11-995-2011

Shoenfelt, E. M., Sun, J., Winckler, G., Kaplan, M. R., Borunda, A. L., Farrell, K. R., et al. (2017). High particulate iron(II) content in glacially sourced dusts enhances productivity of a model diatom. *Sci. Adv.* 3:e1700314. doi: 10.1126/sciadv.1700314

Sohm, J., Webb, E., and Capone, D. G. (2011). Emerging patterns of marine nitrogen fixation. *Nat. Rev. Microbiol.* 9, 499–508. doi: 10.1038/nrmicro2594

Spokes, L. J., and Jickells, T. D. (1996). Factors controlling the solubility of aerosol trace metals in the atmosphere and on mixing into seawater. *Aquat. Geochem.* 1, 355–374. doi: 10.1007/bf00702739

Stucki, J. W., Goodman, B. A., and Schwertmann, U. (2012). *Iron in Soils and Clay Minerals*. Berlin: Springer Science & Business Media, 217.

Suter, D., Banwart, S., and Stumm, W. (1991). Dissolution of Hydrous Iron(III) oxides by reductive mechanisms. *Langmuir* 7, 809–813. doi: 10.1021/la00052a033

Tagliabue, A., Bowie, A. R., Boyd, P. W., Buck, K. N., Johnson, K. S., and Saito, M. A. (2017). The integral role of iron in ocean biogeochemistry. *Nature* 543, 51–59. doi: 10.1038/nature21058

Torfstein, A., Teutsch, N., Tirosh, O., Shaked, Y., Rivlin, T., Zipori, A., et al. (2017). Chemical characterization of atmospheric dust from a weekly time series in the north Red Sea between 2006 and 2010. *Geochim. Cosmochim. Acta* 211, 373–393. doi: 10.1016/j.gca.2017.06.007

Tovar-Sanchez, A., Sañudo-Wilhelmy, S. A., Kustka, A. B., Agustí, S., Dachs, J., Hutchins, D. A., et al. (2006). Effects of dust deposition and river discharges on trace metal composition of Trichodesmium spp. in the tropical and subtropical North Atlantic Ocean. *Limnol. Oceanogr.* 51, 1755–1761. doi: 10.4319/lo.2006.51.4.1755

Trick, C. G. (1989). Hydroxamate -siderophore production and utilization by marine eubacteria. *Curr.Microbiol.* 18, 375–378. doi: 10.1007/s12010-012-9926-y

Velasquez, I. B., Ibisanmi, E., Maas, E. W., Boyd, P. W., Nodder, S., and Sander, S. G. (2016). Ferrioxamine siderophores detected amongst iron binding ligands produced during the remineralization of marine particles. *Front. Mar. Sci.* 3:172. doi: 10.3389/fmars.2016.00172

Villareal, T. A., and Carpenter, E. J. (2003). Buoyancy regulation and the potential for vertical migration in the oceanic cyanobacterium Trichodesmium. *Microb. Ecol.* 45, 1–10. doi: 10.1007/s00248-002-1012-5

Visser, F., Gerringa, L. J. A., Van Der Gaast, S. J., De Baar, H. J. W., and Timmermans, K. R. (2003). The role of the reactivity and content of iron of aerosol dust on growth rates of two Antarctic diatom species. *J. Phycolo.* 39, 1085–1094. doi: 10.1111/j.0022-3646.2003.03-023.x

Wagener, T., Pulido-Villena, E., and Guieu, C. (2008). Dust iron dissolution in seawater: results from a one-year time-series in the Mediterranean Sea. *Geophys. Res. Lett.* 35, 1–6.

Waite, T. D., and Morel, F. M. M. (1984). Photoreductive dissolution of colloidal iron oxides in natural waters. *Environm. Sci. Technol.* 18, 860–868. doi: 10.1021/es00129a010

Walsby, A. E. (1978). The properties and buoyancy-providing role of gas vacuoles in Trichodesmium Ehrenberg. *Br. Phycol. J.* 13, 103–116. doi: 10.1080/00071617800650121

Walter, M., Kraemer, S. M., and Schenkeveld, W. D. C. (2017). The effect of pH, electrolytes and temperature on the rhizosphere geochemistry of phytosiderophores. *Plant Soil* 418, 5–23. doi: 10.1007/s11104-017-3226-9

Walter, M., Schenkeveld, W. D. C., Reissner, M., Gille, L., and Kraemer, S. M. (2019). The effect of ph and biogenic ligands on the weathering of chrysotile asbestos: the pivotal role of tetrahedral fe in dissolution kinetics and radical formation. *Chem. A Eur.J.* 25, 1–16. doi: 10.1002/chem.201804319

Wang, Z., Schenkeveld, W. D. C., Kraemer, S. M., and Giammar, D. E. (2015). Synergistic effect of reductive and ligand promoted dissolution of goethite. *Environ. Sci. Technol.* 49, 7236–7244. doi: 10.1021/acs.est.5b01191

Westberry, T. K., and Siegel, D. A. (2006). Spatial and temporal distribution of Trichodesmium blooms in the world's oceans. *Glob. Biogeochem.Cycles* 20, 1–13.

Whooley, M. A., and McLoughlin, A. J. (1982). The regulation of pyocyanin production in *Pseudomonas aeruginosa*. *Eu. J.Appl. Microbiol. Biotechnol.* 15, 161–166. doi: 10.1007/bf00511241

Wieland, E., and Stumm, W. (1992). Dissolution kinetics of kaolinite in acidic aqueous solutions at 25°C. *Geochim. Cosmochim. Acta* 56, 3339–3355. doi: 10.1016/0016-7037(92)90382-s

Witter, A. E., Hutchins, D. A., Butler, A., and Luther, G. W. (2000). Determination of conditional stability constants and kinetic constants for strong model Fe-binding ligands in seawater. *Mar. Chem.* 69, 1–17. doi: 10.1016/s0304-4203(99)00087-0

Yoshida, T., Hayashi, K. I., and Ohmoto, H. (2002). Dissolution of iron hydroxides by marine bacterial siderophore. *Chem. Geol.* 184, 1–9. doi: 10.1016/s0009-2541(01)00297-2

Young, R. A. (1993). The rietveld method. *Int. Union Crystallogr.* 5, 1–39.

Conflict of Interest: The authors declare that the research was conducted in the absence of any commercial or financial relationships that could be construed as a potential conflict of interest.